Title

Sensitivity to direction and velocity of fast frequency chirps in the inferior colliculus of awake rabbit

Abbreviated Title

Frequency-chirp direction and velocity sensitivity in IC

Paul W. Mitchell[a], Kenneth S. Henry[a,b,c], and Laurel H. Carney[a,b]

[a]Departments of Biomedical Engineering, [b]Neuroscience, and [c]Otolaryngology, University of Rochester, Rochester, NY USA

Corresponding author

Laurel H. Carney, Laurel_Carney@URMC.rochester.edu

Abstract

Neurons in the mammalian inferior colliculus (IC) are sensitive to the velocity (speed and direction) of fast frequency chirps contained in Schroeder-phase harmonic complexes (SCHR). However, IC neurons are also sensitive to stimulus periodicity, a prominent feature of SCHR stimuli. Here, to disentangle velocity sensitivity from periodicity tuning, we introduced a novel stimulus consisting of aperiodic random chirps. Extracellular, single-unit recordings were made in the IC of Dutch-belted rabbits. Periodicity tuning was characterized using modulation transfer functions (MTFs). The prevalence of direction selectivity to SCHR and aperiodic chirps was quantified, demonstrating that the majority of IC neurons (90.5%) were selective for SCHR-chirp direction and that nearly all neurons were selective for aperiodic-chirp direction (99.6%). Rate-

velocity functions were constructed from aperiodic chirp responses, revealing that neurons were commonly sensitive to the direction of lower-velocity (0.40 – 1.59 kHz/ms) chirps and were often insensitive to the direction of higher-velocity chirps (3.16 – 9.24 kHz/ms). Rate-velocity functions and MTFs were combined using a generalized linear model to predict SCHR response rates—this analysis revealed that both velocity and periodicity cues were required to explain SCHR responses. In general, velocity cues had a stronger effect on responses for harmonic stimuli with lower fundamental frequencies. This result has implications for neural encoding of complex sounds that combine envelope periodicities and frequency-sweeps, such as speech.

1. Introduction

The inferior colliculus (IC) receives convergent excitatory and inhibitory inputs from several auditory brainstem nuclei, resulting in a variety of complex response properties including frequency tuning (Davis, 2005), sensitivity to interaural differences (Yin et al., 2019), duration tuning (Casseday et al., 1994), and tuning to amplitude modulation (AM) (Langner and Schreiner, 1988; Krishna and Semple, 2000). Sensitivity of IC neurons to the speed and direction of frequency sweeps has also been studied. Studies of bat IC responses report neurons that prefer, or even respond exclusively to, a particular sweep direction, a possible adaptation for echolocation (Suga, 1965; Fuzessery, 1994; Fuzessery and Hall, 1996; Gordon and O'Neill, 1998; Pollak et al., 2011). Additionally, sounds with statistics resembling vocal spectral-peak transitions have been used to produce IC spectrotemporal receptive fields (STRFs) in cats and bats (Escabí and Schreiner, 2002; Escabí et al., 2003; Andoni et al., 2007).

Recently, IC sensitivity to the velocity (speed and direction) of sweeps has been explored in anesthetized gerbils (Steenken et al., 2022) and awake budgerigars (Henry et al., 2023). These studies used Schroeder-phase (SCHR) harmonic complexes, an advantageous stimulus for studying frequency sweep sensitivity. The harmonic components of SCHR stimuli have flat magnitude spectra and curved phase spectra that create acoustic waveforms with

maximally flat temporal envelopes (Schroeder, 1970). The phase differences across harmonic components result in linear frequency sweeps within each fundamental period, extending from the lowest component, typically the fundamental frequency (F0), to the highest harmonic component. SCHR sensitivity is notable for the sheer speed of its frequency sweeps, which travel from F0 to the maximum harmonic (here, 16 kHz) over the fundamental period (here, between 2.5 and 20 ms). The resulting velocities are faster than commonly considered frequency-modulated signals, such as formant transitions (Liberman and Mattingly, 1989). In this study, we report sensitivity in rabbit IC to the velocity (speed and direction) of these fast SCHR sweeps, referred to here as SCHR chirps. Rabbits do not produce specialized vocalizations containing chirps (Awan et al., 2014) and therefore presumably lack unusual adaptations for processing them. Instead, rabbits have representative mammalian hearing, with average high-frequency audiometric thresholds compared to similarly-sized mammals, and low-frequency thresholds similar to humans (Heffner and Masterson, 1980) – these qualities make the rabbit a good model to ask questions about general chirp sensitivity that may exist in typical mammalian auditory systems.

IC sensitivity to SCHR chirps is poorly understood. Differences in rate in response to SCHR chirps with different directions may be partially explained by the phase-dispersive properties of the cochlea (Recio and Rhode, 2000), which might combine with cochlear compression to result in reduced responses to downward-sweeping SCHR chirps, as observed in the auditory nerve (AN), at least for high-frequency responses (Recio, 2001). Chirp selectivity in the IC could also arise in the cochlear nucleus. For example, octopus cells of the posteroventral cochlear nucleus are selective for SCHR chirp direction (Lu et al., 2022) and provide inhibition to the IC via the ventral nucleus of the lateral lemniscus (Adams, 1997). Alternatively, chirp selectivity may originate (or be influenced) at the level of the IC by the same or similar mechanisms that give rise to other complex stimulus sensitivities. For instance, IC

tuning for stimulus periodicity (Langner and Schreiner, 1988; Krishna and Semple, 2000; Nelson and Carney, 2007; Kim et al., 2020) can be explained by the dynamics of inhibitory inputs (Nelson and Carney, 2004).

A key limitation in our understanding of IC chirp processing is whether stimulus periodicity is necessary to facilitate velocity sensitivity. Studies have often made use of SCHR stimuli, but these stimuli provide a prominent periodicity cue that confounds the purported sensitivity to velocity. Therefore, a new approach is required to disentangle the effects of periodicity tuning from velocity sensitivity on responses to SCHR chirps. In this study, we recorded IC responses to both periodic SCHR stimuli and aperiodic random chirp stimuli to assess velocity sensitivity. From the aperiodic chirp responses, we constructed rate-velocity functions, which describe the sensitivity to velocity of individual neurons. We also used generalized linear models to predict SCHR-chirp responses based on responses to aperiodic chirp stimuli and sinusoidally amplitude-modulated noise and showed that, for most neurons, both periodicity and velocity cues were necessary to accurately predict neural responses to SCHR stimuli.

2. Methods

Extracellular, single-unit recordings were made in the central nucleus of the IC (ICC) of six female Dutch-belted rabbits (*Oryctolagus cuniculus*). Rabbits were obtained from Envigo (Denver, PA). The age of the animals during experiments ranged from 1-5 years, during which distortion-product otoacoustic emissions (DPOAEs) and IC neural thresholds were used to confirm normal hearing (Whitehead et al., 1992). Animals were housed in separate cages in the same room, with a 12-hour light cycle from 6 AM to 6 PM. Animals were removed from the study when their DPOAE magnitudes decreased or neural thresholds increased. All methods were approved by the University of Rochester Committee on Animal Resources.

2.1. Recordings

Recordings were made in daily two-hour sessions between 9 AM and 4 PM in sound-attenuated booths (Acoustic Systems, Austin, TX, USA). To prevent head movement of the awake rabbits, a headbar (metal or 3D-printed plastic) was surgically affixed to the skull using stainless-steel screws and dental acrylic. Rabbits were anesthetized using ketamine (66 mg/kg) and xylazine (2 mg/kg), administered intramuscularly, for headbar placement, craniotomy, and electrode placements (below). Rabbits were wrapped in a towel and secured in a custom-made chair to limit movement during recording sessions.

Recordings were made using four tetrodes, each consisting of four 18-μm platinum-iridium epoxy-coated wires (California Fine Wire Co., Grover Beach, CA, USA) and plated with platinum black to obtain impedances of approximately 0.1 – 0.5 MOhms. Tetrodes were surgically implanted in the ICC via a small (~2-mm diameter) craniotomy in the top of the skull. Stainless-steel guide tubes protected the tetrodes, which were positioned just dorsal to the ICC and then advanced through the ICC using a manual microdrive (Five-drive, Neuralynx, Inc., Bozeman, MT, USA). Tetrodes were advanced before or after recording sessions. The microdrive and tetrodes were surgically replaced every few months, as needed, to vary the recording location. Neural recordings were made using an RHD recording system (Intan Technologies, LLC., Los Angeles, CA, USA), with Intan software running on a Windows PC.

Stimuli were generated using custom MATLAB code (Mathworks, Natick, MA, USA), a MOTU audio interface (16A, Mark of the Unicorn, Cambridge, MA, USA), and a Benchmark digital-to-analog converter and amplifier (DAC3 HGC, Benchmark Media Systems, Inc., Syracuse, NY, USA). Etymotic ER2 earphones (Etymotic Research, Inc., Elk Grove Village, IL, USA) were used to present sound stimuli via custom ear molds (Hal-Hen Company, Inc., Garden City Park, New York, USA). Prior to every session, stimuli were calibrated using ER-7C probe-tube or ER-10B+ microphones (Etymotic Research, Inc., USA). The calibration curve

(magnitude and phase) was included in a pre-emphasis filter that compensated all stimuli for the acoustic system's frequency response.

Action potential times and waveforms were extracted from neural recordings using custom MATLAB applications. To identify single-unit events, the voltage recording was filtered using a 4th-order Butterworth bandpass filter (300 – 3000 Hz). An action potential was identified when the filtered voltage signal exceeded a threshold, defined as four standard deviations of the voltage signal. Action potentials were sorted into clusters, presumed to represent different neurons, using features of the waveforms, primarily the slope of the waveform repolarization (Schwarz et al., 2012). Single-units were identified when less than 2% of the interspike intervals were shorter than 1 ms. Neurons studied in consecutive sessions were considered to be unique only when both tetrode location and response properties changed.

2.2. Stimuli

Recording sessions began by presenting wideband (100 Hz – 15 kHz) noise to the two ears to characterize the binaural responses. Noise stimuli were presented to the contralateral ear, ipsilateral ear, and both ears at 3, 13, and 33 dB SPL spectrum level, with 1-s durations and 3 repetitions each. Then, a set of stimuli was presented to define neural response properties, including frequency response maps, modulation transfer functions, SCHR sensitivity, and rate-velocity functions.

To generate frequency response maps, a randomly-ordered sequence of 0.2-s-duration tones at frequencies ranging from 250 Hz – 16 kHz was presented at 13, 33, 53, and 73 dB SPL. Tones were presented either contralaterally or diotically with 10-ms raised-cosine on/off ramps, and were separated by 0.4 s of silence. Each stimulus condition was presented three times. Response maps, plots of average discharge rate vs. frequency at each stimulus level,

were used to estimate characteristic frequency (CF), the frequency for which threshold was lowest.

Modulation transfer functions (MTFs) were estimated by computing the average rate in response to 100% sinusoidally amplitude-modulated noise as a function of modulation frequency, over a range of 2 – 350 Hz. The wideband noise (100 Hz – 10 kHz) was 1 s in duration, including 50-ms raised-cosine on/off ramps, presented diotically. Modulation frequencies were presented in random order, with 5 repetitions of each. Noise presentations were separated by 0.5 s of silence. Stimuli were presented at a spectrum level of 33 dB (overall level of 73 dB SPL). MTF categorization was based on criteria that were slightly modified from Kim et al. (2020). MTF types were categorized as band-enhanced (BE) if (1) the MTF had two consecutive points greater than the product of the unmodulated rate (r_{um}) and a criterion K, and (2) the MTF did not have more than one point below the product of r_{um} and $1/K$. Similarly, MTFs were categorized as band-suppressed (BS) if (1) the MTF had two consecutive points less than r_{um}/K, and (2) the MTF did not have more than one point above $r_{um} \times K$. For this study, K was set to 1.2, i.e., a 20% increase in rate with respect to the unmodulated response was required for BE MTFs and a 20% decrease was required for BS MTFs. MTFs that had both enhanced and suppressed bands that met the above criteria were categorized as hybrid MTFs. In the population of neurons studied, 43.3% were BS, 17.0% were BE, 24.5% were hybrid, 5.2% were flat, and the rest had other MTF shapes including high-pass or low-pass.

SCHR stimuli were produced using the phase spectrum introduced in Schroeder (1970) (Fig. 1A-D). For a harmonic complex with n components, the phase of the nth component was

described by $\theta_n = C\pi n(n+1)/N$, where N is the total number of harmonic components, and C

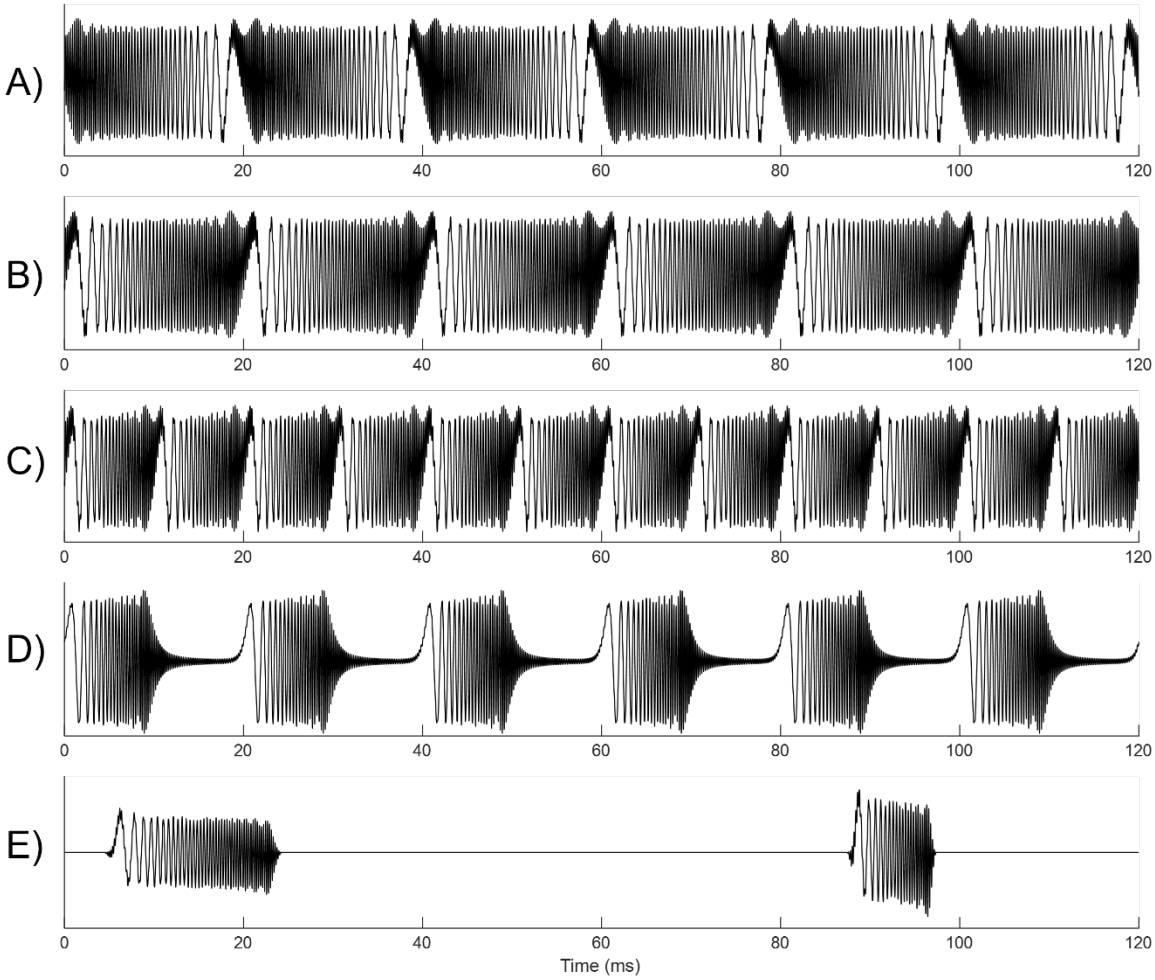

Figure 1 – Stimulus waveforms of SCHR and aperiodic chirp stimuli. Note that the maximum harmonic in this figure is 5 kHz for clarity; in the actual stimuli, maximum harmonic was 16 kHz. (A) Downward SCHR with F0 = 50 Hz, C = +1. (B) Upward SCHR with F0 = 50 Hz, C = -1. (C) Upward SCHR with F0 = 100 Hz, C = -1. (D) Upward SCHR with F0 = 50 Hz, C = -0.5. (E) Two consecutive aperiodic chirps separated by silence.

is a scalar that describes the phase-direction and duty cycle of the stimulus. For simplicity, SCHR stimuli with a positive C-value will be referred to as downward SCHR, reflecting the direction of their frequency chirps. SCHR stimuli with a negative C-value will be referred to as upward SCHR. Note that the direction of SCHR chirp (upward or downward) is the opposite of its phase (negative or positive, respectively). A random sequence of SCHR stimuli was presented, with F0 equal to 50, 100, 200, or 400 Hz, and C equal to -1, -0.5, 0, 0.5, or 1. For all

cases, the frequency of the highest harmonic component was 16 kHz. The number of harmonic components, N, depended on F0, and ranged between 40 and 320. Thirty repetitions of each F0 and C combination were presented. Stimuli were presented diotically at 63 dB SPL, with a duration of 0.4 seconds, 0.6 seconds of silence between stimuli, and 25-ms raised cosine on/off ramps. Average discharge rates over the stimulus duration were calculated for each F0 and C combination. Receiver-operating-characteristic (ROC) analysis (Egan, 1975) was used to evaluate neural direction selectivity for SCHR conditions with equivalent F0 and C-values of opposite signs (i.e. F0 = 50 Hz, C = ±1). Neurons were deemed significantly biased toward one sweep direction if the ROC area under the curve (AUC) was above 70.7% or below 29.3%. Neurons with AUCs above 70.7% were designated as selective for upward chirps (indicating greater mean response rate) and neurons with AUCs below 29.3% were designated as selective for downward chirps. The ROC thresholds of 70.7% and 29.3% were chosen because they are equivalent to the targeted threshold of two-down, one-up psychophysical procedure (Levitt, 1971).

Rate-velocity functions (RVFs) were solely based on responses to aperiodic chirp stimuli. Aperiodic chirp stimuli consisted of isolated SCHR chirps, or single fundamental periods extracted from a SCHR stimulus, equivalent to one full SCHR chirp spanning F0 to the maximum harmonic, or vice versa (Fig. 1E). To produce the stimulus waveforms, first, we generated a random sequence of chirp velocities that were equivalent to SCHR F0s of 25, 50, 100, 200, 400, and 600 Hz. Chirp direction (upward or downward) was also randomly varied across stimuli. These parameters together resulted in aperiodic chirps with velocities ±0.40, ±0.80, ±1.59, ±3.16, ±6.24, and ±9.24 kHz/ms. Each combination of velocity and direction was presented a total of 42 times within each full stimulus, in random order. To avoid periodicity, chirps were randomly spaced, using 40 – 60 ms uniformly distributed inter-chirp intervals. The full stimulus set was presented 20 times. Each individual chirp had raised-cosine on/off ramps,

each with duration equivalent to 10% of chirp duration. Chirps were presented diotically at a sound level equal to $68\ dB\ SPL - 10 \times \log_{10}(T/T_{ref})$, where T is the duration of the chirp, and T_{ref} = 2.5 ms (the duration of a SCHR chirp with F0 = 400 Hz). This scaling ensured that energy was equivalent across chirps of different durations. Extracting response rates from aperiodic chirp responses was complicated by variation in onset response latency and the presence of offset responses in many neurons. The response-rate calculation began by locating the peak rate in the peristimulus time histogram (PSTH) over a time window starting at chirp onset with a duration matched to that of the chirp plus the minimum spacing between chirps (i.e., chirp duration + 40 ms) (Fig. 2). Then, response rate was calculated by summing spikes over a 20-ms time window centered at the peak of the PSTH, except where this window would cross the minimum (0 ms) or maximum (chirp duration + 40 ms) of the PSTH time axis. ROC analysis of aperiodic chirp rates was performed in an identical manner as for SCHR rates. Aperiodic chirp rates were used to generate RVFs, which described how a neuron's rate changed as a function of chirp velocity (Figs. 3-7).

2.3. Analysis

Principal Component Analysis (PCA) was performed on the RVFs using the MATLAB function PCA (2021b, MathWorks) on the set of RVFs (247 in total). RVFs were normalized by their individual peak rates before PCA analysis. SCHR responses were predicted based on MTFs and RVFs using generalized linear models (GLMs) (Nelder and Wedderburn, 1972). First,

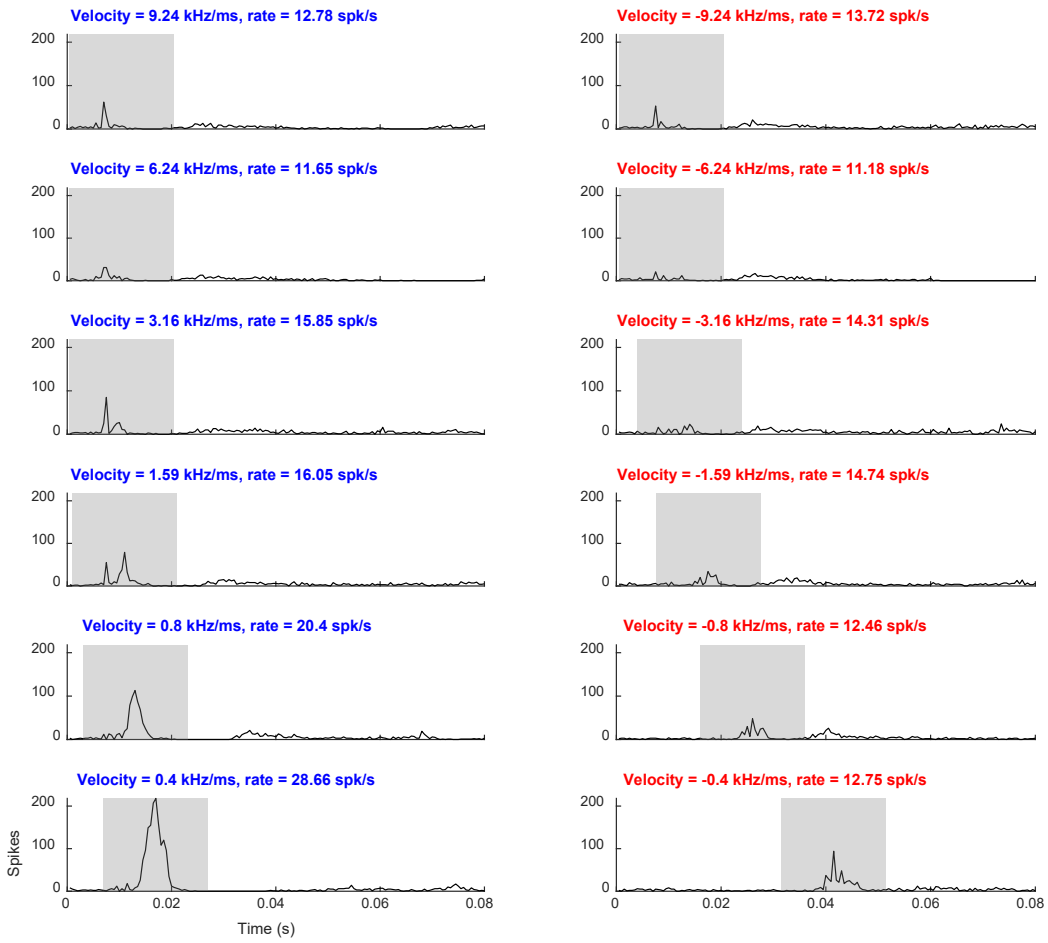

Figure 2 – A visual depiction of aperiodic chirp stimulus rate calculation. Black lines illustrate PSTHs (bin size = 0.5 ms) of responses to chirps of different velocities. The left column (blue titles) contains upward chirps, and the right column (red titles) contains downward chirps. The shaded rectangles indicate the placement of the 20-ms window over which response rate is calculated. The window is centered at the peak of the PSTH, except where that would cause the window to cross the minimum (0 ms) or maximum (chirp duration + 40 ms) time intervals (e.g. velocity = 9.24 kHz/ms PSTH, top left).

SCHR rates, MTFs, and RVFs were normalized by each of their maximum rates. For the responses to periodic stimuli, (MTF and SCHR), cycle rate was used, defined as the average rate per fundamental period. Cycle rate (spikes/cycle) was used to counteract the strong phase-locking of many neurons to the fundamental frequency, which resulted in average rates that disproportionally increased with F0 using the conventional calculation (spikes/second). For the aperiodic chirp stimulus, rate was calculated using the previously mentioned method of

summing spikes over a window up to 40-ms in duration centered around the peak of the PSTH. The periodicity and velocity of each SCHR point was matched with the closest available modulation frequency and velocity from the MTF and RVF, respectively (data were not interpolated), creating a feature vector for the neurons' pure response to periodicity and velocity changes. Then, a relationship between the periodicity and velocity feature vectors and SCHR rates was defined for the GLM as follows:

$$R_S = b_P R_P + b_V R_V + b_I (R_P * R_V) + b_0 \quad , \qquad \text{(Eqn. 1)}$$

where R_P and R_V refer to rates of the periodicity and velocity feature vectors, respectively. R_S is the predicted response to SCHR stimuli in cycle rate, and b_n are the GLM coefficients. There were three terms in the GLM—a periodicity term, a velocity term, and an interaction term. GLM coefficients were estimated using the MATLAB function glmfit (2021b, MathWorks), with the distribution argument set to *normal* and constant argument set to *on*. The GLM coefficients were b_P, the periodicity coefficient, b_V, the velocity coefficient, b_I, the interaction term coefficient, and b_0, a constant. After the SCHR rate prediction was calculated using estimated coefficients, the coefficient of determination (R^2) of the predicted and recorded SCHR cycle rates was determined to assess prediction quality. This process was repeated for two additional, simpler GLMs:

$$R_S = b_1 R_P + b_0 \quad , \text{ and} \qquad \text{(Eqn. 2)}$$

$$R_S = b_1 R_V + b_0 \quad . \qquad \text{(Eqn. 3)}$$

These simpler GLMs depended only on one feature vector and thus could be used to assess the importance of periodicity or velocity alone. The coefficients of determination (R^2) of these two model predictions were obtained and used to measure the impact of the two features on neurons' SCHR responses.

The following equation was used to calculate the contribution of velocity-cues to the total explainable variance:

$$Percent\ contribution\ of\ velocity\ to\ R^2 = \frac{\left(R^2{}_{combined} - R^2{}_{periodicity}\right)}{R^2{}_{combined}} \times 100\ , \qquad \text{(Eqn. 4)}$$

where $R^2{}_{combined}$ and $R^2{}_{periodicity}$ refer to the coefficient of determination of the combined model (Eqn. 1) and periodicity-alone model (Eqn. 2), respectively. Equation 4 allowed the amount of additional variance explained by the inclusion of velocity (either in the velocity term or interaction term in Eqn. 1) to be directly quantified.

3. Results

3.1. Sensitivity of IC neurons to velocity of SCHR chirps was diverse

Data were recorded over a span of 330 sessions and included recordings from 335 unique single units. Response properties of single-unit neurons are illustrated using response maps, MTFs, RVFs, and raster plots of SCHR responses (Figs. 3-7). Neural sensitivity to chirps is often evident in SCHR raster plots, which illustrate detailed timing and rate differences in response to different velocities of SCHR stimuli. Response maps were used to determine CF; these plots also reveal off-CF inhibitory regions. MTFs were categorized by shape (i.e., BE, BS, hybrid). Lastly, RVFs were constructed from aperiodic chirp responses. Unlike the SCHR raster plots, RVFs reflect velocity sensitivity removed from a periodic context. Altogether, response maps, MTFs, and RVFs defined each neuron's response profile to basic sound features. Response profiles were examined to assess the relative importance of feature sensitivities on SCHR responses, including modulation tuning, off-CF inhibition, and chirp velocity tuning.

Figure 3 shows an example of a unit with a complex SCHR response that was not fully explainable by the responses to characterizing stimuli. The SCHR dot raster plot (Fig. 3C) displays stronger rates in response to downward SCHR (red dots) at the lowest-velocity chirp pair (50 Hz, C = ±1). This downward SCHR preference was not maintained for higher velocities.

The neuron's MTF (Fig. 3B) was BS, with a trough spanning modulation frequencies that included the SCHR F0s of 50 and 100 Hz, and with relatively less suppression at modulation frequencies matching the F0s of 200 and 400 Hz. If the MTF solely predicted this neuron's SCHR response, responses to 50- and 100-Hz SCHR chirps should have been nearly entirely suppressed. However, the neuron's response was robust for all 50-Hz chirp conditions except for 50 Hz, C = -1, suggesting that the direction and/or velocity sensitivity to these chirps overcame the suppression observed in the MTF. Thus, the MTF alone could not simply explain this neuron's SCHR response profile. Meanwhile, the response map (Fig. 3A) was sharply tuned

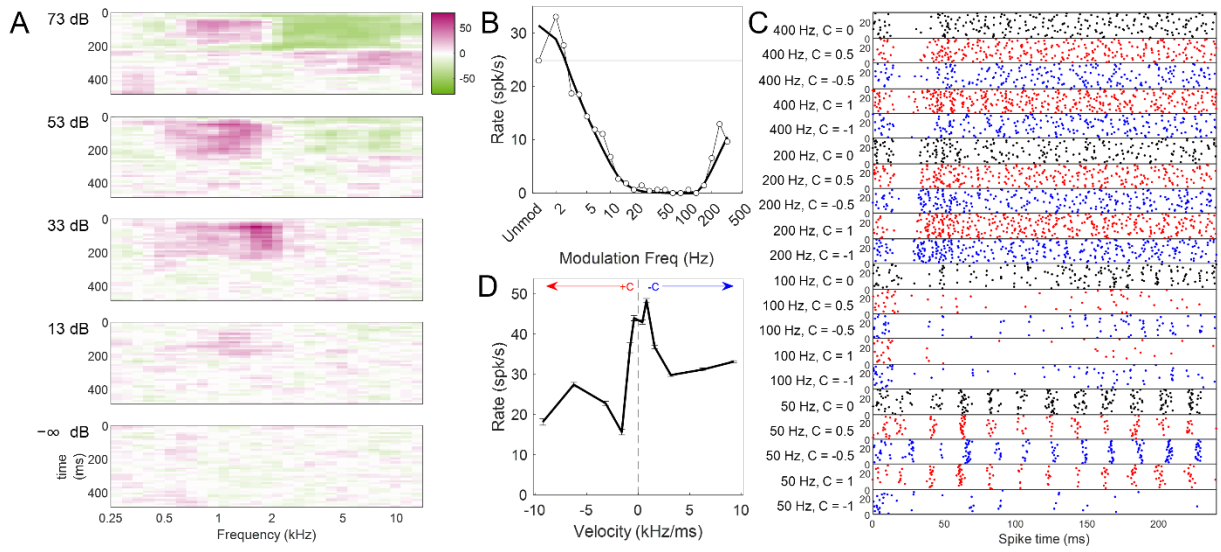

Figure 3 – Responses of unit R24TT4P7N2 to characterizing stimuli. (A) Response Map – Panels are arranged vertically by sound level of pure tones. Color plots reflect response rate versus frequency (x-axis) and time following tone onset (y-axis); magenta regions have increased activity relative to spontaneous rate, and green regions have decreased activity relative to spontaneous rate. (B) Modulation Transfer Function – rate versus modulation frequency. The solid black line is smoothed from raw data (shown as circular points). Grey horizontal line reflects unmodulated rate. (C) Dot raster plots of SCHR responses – Panels are arranged vertically by SCHR condition (F0 and C-value pairs). Within panels, rows of dots reflect repetitions (30 each). Responses to upward SCHR are plotted with blue dots, and downward SCHR with red dots. Black is used for C = 0. For rows with C = ±1, F0s of 50, 100, 200, and 400 Hz correspond to chirp velocities of ±0.80, ±1.59, ±3.16, and ±6.24 kHz/ms, respectively. For rows with C = ±0.5, F0s of 50, 100, 200, and 400 Hz correspond to chirp velocities of ±1.59, ±3.18, ±6.32, and ±12.48 kHz/ms, respectively. For rows with C = 0, chirp velocity was infinite. (D) Rate-velocity function – constructed using responses to aperiodic chirp stimuli. Colored arrows mark the SCHR C-values of chirps of equivalent direction. Error bars are the standard error of rates across repetitions (20 each).

to 1.2 kHz with a low threshold (13 dB SPL), and revealed a high-frequency inhibitory region at high sound levels with a long duration and shorter latency than the excitation at CF. If the neuron's SCHR response were dependent on this asymmetrical sideband inhibition, the long-duration inhibition would suppress the coincident excitation during downward chirps, resulting in a stronger response to upward chirps than to downward chirps (Gordon and O'Neill, 1998). However, the neuron instead responded more strongly to downward chirps for 50-Hz F0. Therefore, the neuron's asymmetrical sideband inhibition alone could not explain the SCHR response. The neuron's RVF (Fig. 3D) shows an increased response to upward chirps compared to downward chirps for most velocity-pairs (with the exception of ±0.40 kHz/ms). For the most part, the RVF also did not adequately explain SCHR responses; that is, SCHR rates did not consistently favor upward chirps. Instead, direction selectivity was only strong at 50 Hz, C = ±1, showing a selectivity for downward SCHR chirps. This neuron's SCHR response is not explainable by any single response property (as characterized by its response map, MTF, and RVF), and instead was driven by an interaction between response properties.

Another example neuron, illustrated in Fig. 4, had a BE MTF, and a response map dominated by excitation, with a CF of 2 kHz. This neuron's raster plot for SCHR responses showed relatively greater responses to downward chirps for all chirp pairs, with the exception of 400-Hz SCHR stimuli, which were comparatively direction-neutral and notably suppressed relative to other F0s. In contrast, Figure 5 shows responses of an example neuron with a BE MTF and a response map similarly dominated by excitation, with a CF of 2.3 kHz. However, this neuron was selective for upward SCHR for nearly all chirp pairs, with the exception of 400-Hz SCHR. Thus, neurons with the same MTF type could have opposing chirp-direction selectivity. Again, the MTF shape alone did not predict SCHR responses. Additionally, neither of the neurons in Figs. 4 and 5 had response maps with inhibitory regions, although the low spontaneous rates of these neurons likely prevented the response maps from showing

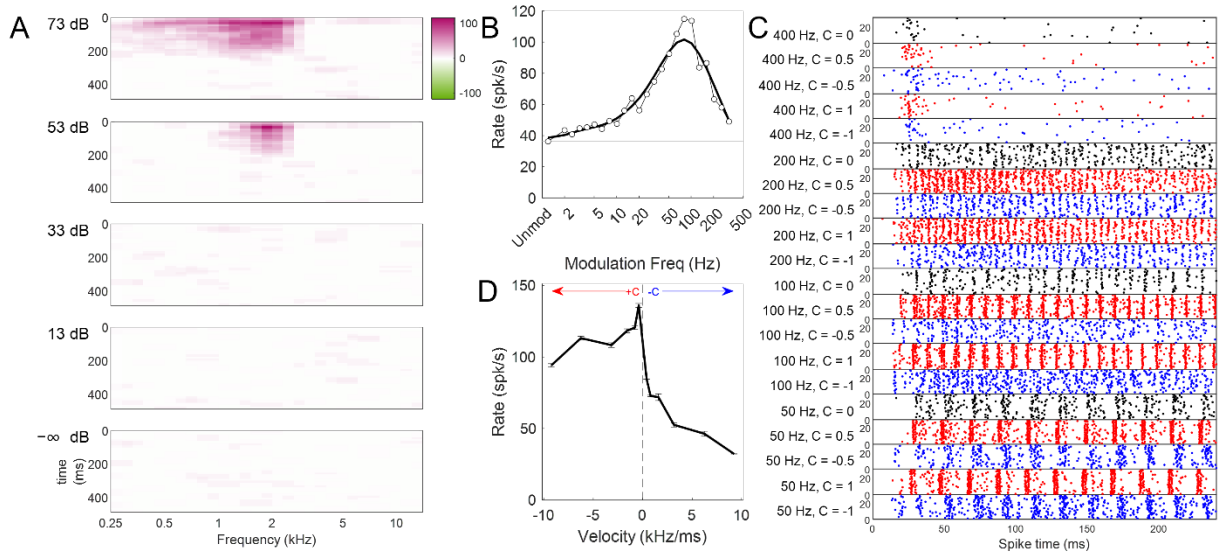

Figure 4 – Responses of unit R24TT2P8N4 to characterizing stimuli. (A) Response Map, (B) Modulation Transfer Function, (C) SCHR dot-raster plot, (D) Rate-Velocity Function. Figure description identical to Fig.3.

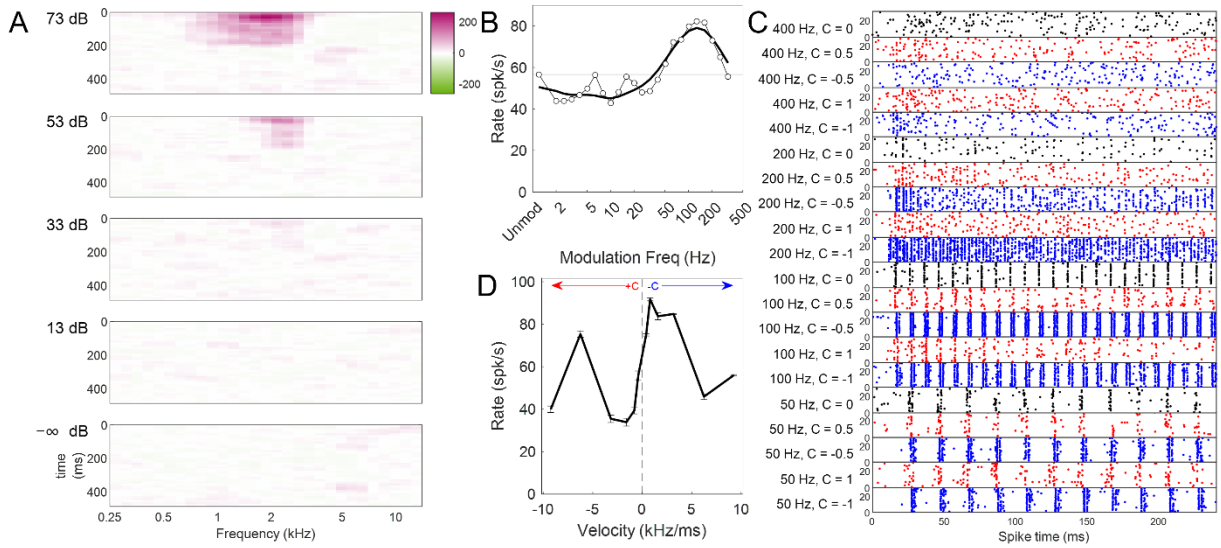

Figure 5 – Responses of unit R25TT2P5N1 to characterizing stimuli. (A) Response Map, (B) Modulation Transfer Function, (C) SCHR-dot raster plot, (D) Rate-Velocity Function. Figure description identical to Fig. 3.

inhibition. However, there was also no evidence for inhibition from either ear based on the neurons' binaural noise responses; for example, adding ipsilateral noise did not suppress responses to contralateral noise. Finally, these neurons both had RVFs that were consistent

with the SCHR rate profiles. In Fig. 4D, downward chirps elicited a higher response rate than upward ones for every velocity-pair. In Fig. 5D, the responses to upward chirps were larger to all velocity-pairs, except for ±6.24 kHz/ms (equivalent to 400 Hz). These examples are neurons in which velocity tuning was highly predictive of SCHR response.

Figure 6 shows responses of a neuron with a flat MTF that was also selective for upward SCHR at low F0s. This figure illustrates that neurons that were neither BE nor BS could still be sensitive to the direction of SCHR chirps, providing further evidence that SCHR sensitivity was not a property tied to a particular MTF type.

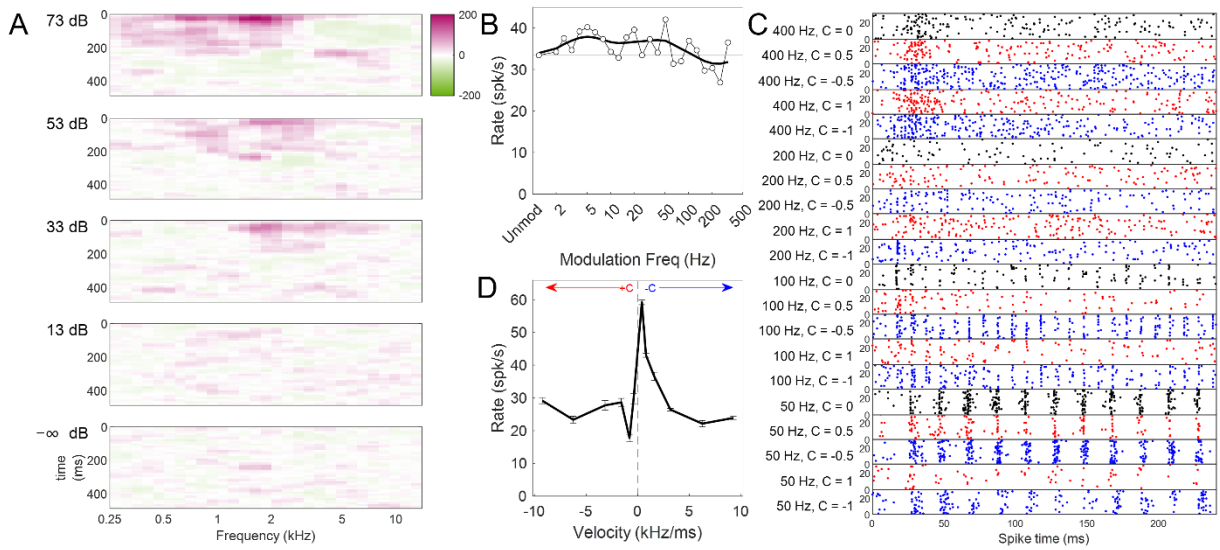

Figure 6 – Responses of unit R24TT2P8N3 to characterizing stimuli. (A) Response Map, (B) Modulation Transfer Function, (C) SCHR dot-raster plot, (D) Rate-Velocity Function. Figure descriptions identical to Fig. 3.

Figure 7 shows responses of an example neuron with a response map that had a low-frequency inhibitory region at high tone levels. This inhibition appears to slightly lag the excitatory region around CF—according to the prediction based on asymmetric inhibition, an upward sweep should result in a coincidence of inhibition and excitation, resulting in selectivity

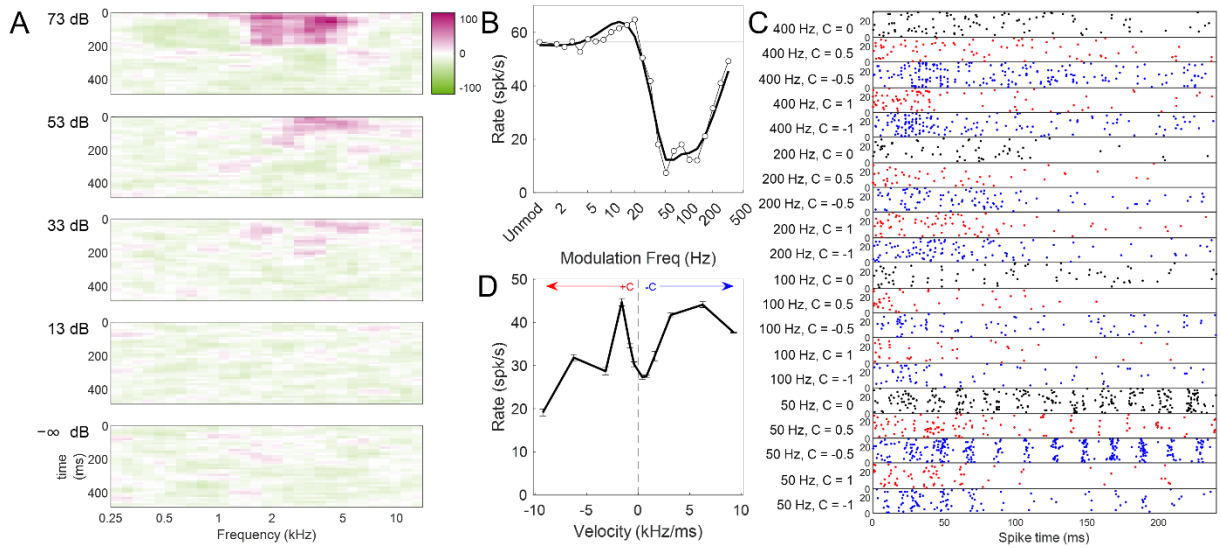

Figure 7 – Responses of unit R24TT1P9N2 to characterizing stimuli. (A) Response Map, (B) Modulation Transfer Function, (C) SCHR dot raster plot, (D) Rate-Velocity Function. Figure description identical to Fig. 3.

towards downward chirps. However, the dot-raster plots of the neuron responses to SCHR stimuli show a selectivity towards upward chirps. Figures 3 and 7 are examples for which chirp selectivity did not agree with the prediction made by the asymmetric inhibitory-sideband theory (Fuzessery and Hall, 1996; Gordon and O'Neill, 1998) and suggest that sideband inhibition alone could not predict SCHR responses.

These example neurons illustrate the diversity of response profiles to SCHR chirps in the IC. Conventional IC features, such as modulation tuning and off-CF inhibition observed in response maps, could not fully explain the responses to SCHR chirps. These observations led to the hypothesis that sensitivity to chirp velocity itself contributed to SCHR-chirp sensitivity. This hypothesis served as the motivation for the aperiodic chirp stimulus, which allowed variation of the velocity cue. RVFs were based on aperiodic chirp responses, and often reflected the rate profiles seen in SCHR dot-raster plots (e.g., Figs. 4,5, and 6), but sometimes did not (e.g., Figs. 3 and 7), suggesting that while many SCHR responses could be explained by their RVFs, others required a more complex interaction between multiple feature sensitivities.

3.2. The majority of IC neurons were selective for SCHR direction

The prevalence of SCHR direction selectivity was quantified for the population of recorded neurons using ROC analysis. SCHR response rates were organized by F0 and C magnitude and grouped by chirp direction (sign of C). Neurons for which response rate allowed direction to be discriminated 70.7% of the time via the ROC test were labeled direction-sensitive.

In total, SCHR responses were recorded from 157 neurons. In Table 1, the *Overall* column shows the percentage of all neurons that were direction selective for each F0 and C condition, or for at least one combination (i.e., Table 1, bottom row). Direction selectivity was

F0 (Hz)	C-Value	Overall (n = 157)	BE (n = 31)	BS (n = 59)	Hybrid (n = 41)	Low CF (n = 36)	Mid CF (n = 39)	High CF (n = 82)
50	±1	53.5	74.2	45.8	51.2	58.3	61.5	47.6
	±0.5	59.2	81.0	47.1	60.0	56.7	73.9	55.6
100	±1	51.0	77.4	44.1	36.6	63.9	61.5	40.2
	±0.5	51.2	66.7	49.0	34.3	50.0	73.9	44.4
200	±1	50.3	67.7	47.5	36.6	63.9	56.4	41.5
	±0.5	35.2	71.4	23.5	22.9	33.3	60.9	27.8
400	±1	49.0	48.4	47.5	51.2	47.2	48.7	50.0
	±0.5	48.8	66.7	41.2	45.7	46.7	56.5	47.2
Any F0 and C-value combination		90.5	93.6	93.2	82.9	97.2	92.3	86.6

Table 1 - Percent of direction sensitive neurons by subgroup as determined by ROC analysis of SCHR responses. Neurons are sorted into subgroups by MTF shape and CF. Neurons with CF less than 6 kHz were labeled "Low CF", and neurons with CF greater than 6 kHz were labeled "High CF". Direction sensitivity was quantified for each F0/C condition. The percentage of neurons sensitive for any F0/C condition was also determined, defined as neurons that were sensitive to sweep direction for at least one F0/C condition.

slightly more common for lower F0s and generally was less common for higher F0s.

For a given F0, the C = ±0.5 condition had a chirp velocity equivalent to C = ±1 for the 2×F0 condition. However, these equivalent-velocity pairs often differed in prevalence of direction selectivity (i.e., 200 Hz, C = ±0.5 and 400 Hz, C = ±1, *Overall* column). This result suggested that prevalence of direction selectivity did not depend solely on chirp velocity and was possibly also influenced by SCHR periodicity or duty cycle.

Finally, 90.5% of neurons were direction selective in at least one F0 and C condition (Table 1, bottom row), demonstrating that SCHR chirp direction selectivity was nearly ubiquitous. To determine the proportion of neurons expected to be selective in at least one SCHR condition by random chance, responses to either direction were shuffled within each C-pair for each neuron. ROC tests were then performed on these shuffled responses, and the neurons that were direction selective for at least one F0/C condition were tallied as before. After shuffling the responses 1000 times, 3.2% of the neurons were selective for at least one F0/C condition (with a standard deviation of 2.6%), suggesting that the threshold used in the ROC test (70.07%) was sufficiently high.

3.3. MTF shape, but not CF, was related to prevalence and direction of SCHR selectivity

The prevalence of SCHR-direction selectivity depended on F0. Hence, it was relevant to quantify the extent to which modulation sensitivity could influence SCHR responses. To examine the effect of MTF shape on SCHR direction selectivity, results of an ROC analysis are shown in Fig. 8. BE neurons were significantly more direction selective than BS neurons for 5 SCHR conditions, and more direction selective than Hybrid neurons for 5 conditions, suggesting that BE neurons were more often direction selective than other MTF shapes (χ^2 test of independence, Fig. 8 caption). Additionally, for several SCHR conditions (e.g., 50 Hz, C = ±1; 50 Hz, C = ±0.5; 400 Hz, C = ±0.5) a notably larger percentage of BE neurons were selective for downward SCHR chirps than for the rest of the MTF shapes. For most SCHR conditions, all

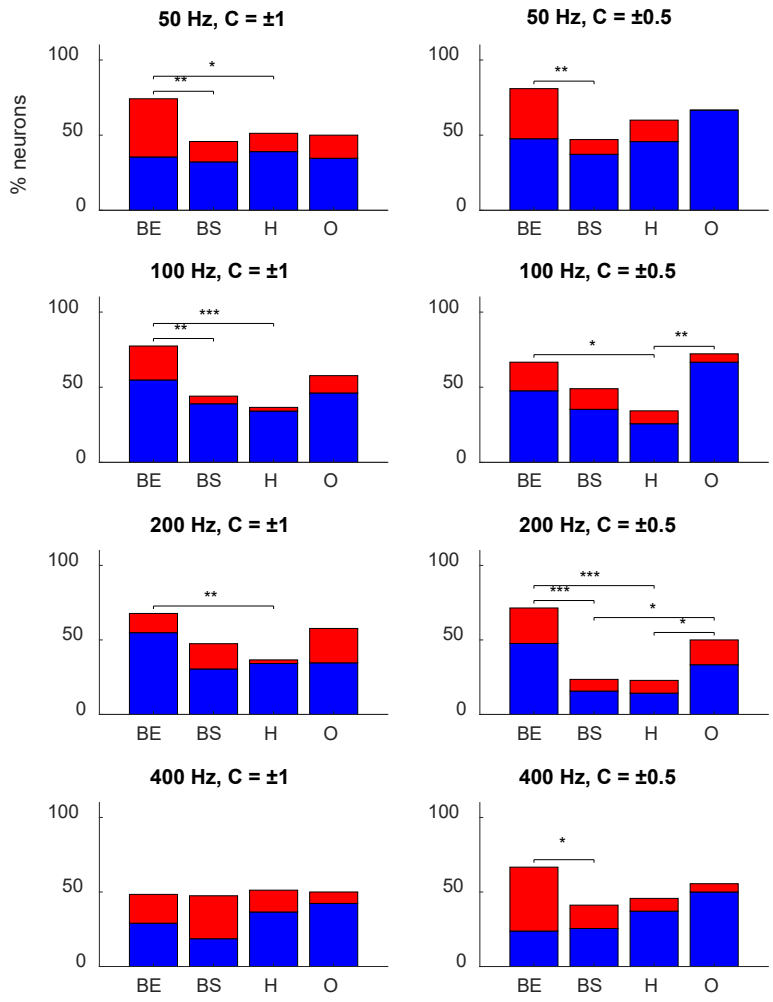

Figure 8 - Percent of direction selective neurons determined by ROC analysis for different MTF shapes, by SCHR condition (BE – Band-Enhanced, BS – Band-Suppressed, H – Hybrid, O – Other). Blue bar-segments represent neurons selective for upward SCHR, and red bar-segments represent neurons selective for downward SCHR. Brackets indicate significant differences of direction selectivity prevalence between groups, as determined by the χ^2 test of independence, with asterisks indicating the level of significance ($p < 0.05$, ** $p < 0.01$, *** $p < 0.001$). Precise p-values are reported here for each panel. 50 Hz, C = ±1—BE-BS, $p = 0.0099$; BE-H, $p = 0.0477$. 50 Hz, C = ±0.5—BE-BS, $p = 0.0083$. 100 Hz, C = ±1—BE-BS, $p = 0.0025$; BE-H, $p = 0.0006$. 100 Hz, C = ±0.5—BE-H, $p = 0.0187$; H-O, $p = 0.0088$. 200 Hz, C = ±1—BE-H, $p = 0.0088$. 200 Hz, C = ±0.5—BE-BS, $p = 0.0001$; BE-H, $p = 0.0003$; BS-O, $p = 0.0359$; H-O, $p = 0.0450$. 400 Hz, C = ±0.5—BE-BS, $p = 0.0492$.*

MTF types tended to be selective for upward chirps. However, for all but one MTF group and SCHR condition (*Other*, 50 Hz, C = ±50 Hz), neurons selective for either direction appeared. Interestingly, despite the large differences between BE and BS groups within individual SCHR conditions, the percentage of neurons in each group that were direction selective in at least one

SCHR condition (Table 1, bottom row) were similar. This result shows that BS neurons were more frequently selective only at a few SCHR conditions compared to BE neurons. Indeed, the average number of selective SCHR conditions among BE neurons was 4.6, compared to 3.2 conditions on average for BS neurons. Hybrid neurons were selective for 3.1 conditions on average. Overall, the prevalence of direction selectivity among BE, BS, and hybrid neurons was high, with hybrid neurons having the lowest prevalence.

To examine the effect of CF on SCHR direction selectivity, results of an ROC analysis for different CF ranges are shown in Fig. 9. The relationship of prevalence of selectivity and CF is less clear than for MTF shape. Generally, low-CF and mid-CF neurons were more often selective than high-CF neurons, but this trend varied by SCHR condition. Generally, more neurons in most CF groups were selective for upward SCHR, for all SCHR conditions. Overall, much like MTF groups, all CF groups had neurons selective for either direction. Also, like the MTF groups, all CF groups had an overall high percentage of direction selectivity (Table 1, bottom row).

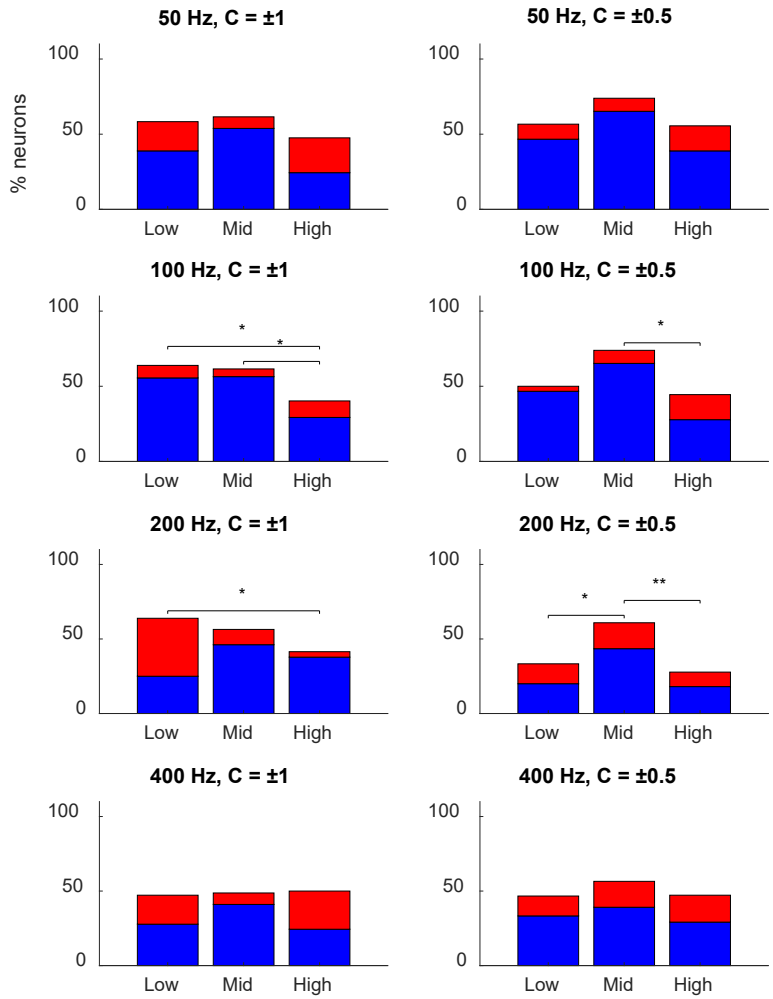

Figure 9 - Percent of direction selective neurons determined by ROC analysis for different CF ranges, low (<3 kHz), mid (>3 kHz and <6 kHz), and high (>6 kHz), by SCHR condition. Blue bar-segments represent neurons selective for upward SCHR, and red bar-segments represent neurons selective for downward SCHR. Brackets indicate significant differences of direction selectivity prevalence between groups, as determined by the χ^2 test of independence, with asterisks indicating the level of significance ($p < 0.05$, ** $p < 0.01$, *** $p < 0.001$). Precise p-values are reported here for each panel. 100 Hz, C = ±1—Low-High, $p = 0.0179$; Mid-High, $p = 0.0283$. 100 Hz, C = ±0.5—Mid-High, $p = 0.0138$. 200 Hz, C = ±1—Low-High, $p = 0.0248$. 200 Hz, C = ±0.5—Low-Mid, $p = 0.0459$; Mid-High, $p = 0.0040$.*

3.4. Direction selectivity to aperiodic chirps was near-ubiquitous

ROC analysis was performed on responses to aperiodic chirp stimuli to determine the prevalence of direction selectivity of neurons in the absence of periodicity. Similar to the analysis performed for SCHR responses (Table 1), aperiodic chirp responses were compared between chirps of equal speed and opposite direction. Pairs for which the chirp direction could be discriminated 70.7% of the time via ROC test were labeled direction-selective.

Aperiodic chirp responses were collected from 247 neurons (Table 2). As for the SCHR ROC results, direction selectivity to aperiodic chirps was common for faster chirp velocities and became increasingly uncommon as velocity increased. When comparing equivalent velocity

Velocity (kHz/ms)	Overall (n = 247)	BE (n = 33)	BS (n = 115)	Hybrid (n = 67)	Low CF (n = 90)	Mid CF (n = 36)	High CF (n = 121)
±0.40	80.2	90.9	80.9	71.6	85.6	86.1	74.4
±0.80	72.9	78.8	72.2	67.2	78.9	69.4	69.4
±1.59	73.3	87.9	73.9	73.1	76.7	75.0	70.2
±3.16	62.3	69.7	53.9	71.6	57.8	55.6	67.8
±6.24	56.3	63.6	53.9	61.2	53.3	38.9	63.6
±9.24	52.2	48.5	47.8	61.2	46.7	52.8	56.2
Any Velocity	99.6	100	100	98.5	100	100	99.2

Table 2 – Percent of direction selective neurons by subgroup as determined by ROC analysis of aperiodic chirp responses. Neurons are sorted into subgroups by MTF shape and CF. Neurons with CF less than 6 kHz were labeled "Low CF", and neurons with CF greater than 6 kHz were labeled "High CF". Direction selectivity was quantified for each F0/C condition. The percentage of neurons selective for any F0/C condition was also determined, defined as neurons for which at least one F0/C condition was selective.

conditions between SCHR and aperiodic chirp responses (e.g. 0.80 kHz/ms aperiodic chirp and 50-Hz SCHR, etc.), neurons were more commonly selective for aperiodic chirps than for their SCHR counterparts. Finally, 99.6% of neurons were direction selective for at least one

aperiodic-chirp velocity (Table 2, bottom row). Stated differently, only one neuron among the 247 surveyed was not significantly direction selective at any velocity. This result demonstrates that neurons were nearly universally direction selective to chirps in aperiodic stimuli.

As for the SCHR ROC analysis, responses to each chirp-direction pair were shuffled for each neuron, and an ROC test was performed on the shuffled responses to ensure that a reasonable threshold was used for determining direction selectivity. Shuffling the responses 1000 times, 13.3% of the neurons were selective for at least one F0/C condition (with a standard deviation of 9.0%). It is clear that the actual percentage of 99.6% could not be due to variance in the data, suggesting that the threshold used in the ROC test (70.07%) was sufficiently high.

3.5. MTF shape and CF were not related to prevalence and direction of aperiodic-chirp selectivity

The results of ROC analysis revealed different trends for aperiodic chirp responses than for SCHR responses. As expected, there was not as pronounced an effect of MTF shape on either the prevalence or direction of aperiodic chirp selectivity (Fig. 10). BE-neuron selectivity was not more prevalent than that of other MTF shapes, as seen for SCHR responses in Fig. 8. Instead, all MTF shapes showed decreasing prevalence of direction selectivity with increasing chirp velocity (Table 2). The direction of aperiodic chirp selectivity changed with chirp velocity as well – at the two slower velocities tested (±0.40 and ±0.80 kHz/ms), neurons were more frequently selective for upward chirps. At the four higher velocities (±1.59 kHz/ms and faster), neurons of all MTF types were more likely to be selective for downward chirps.

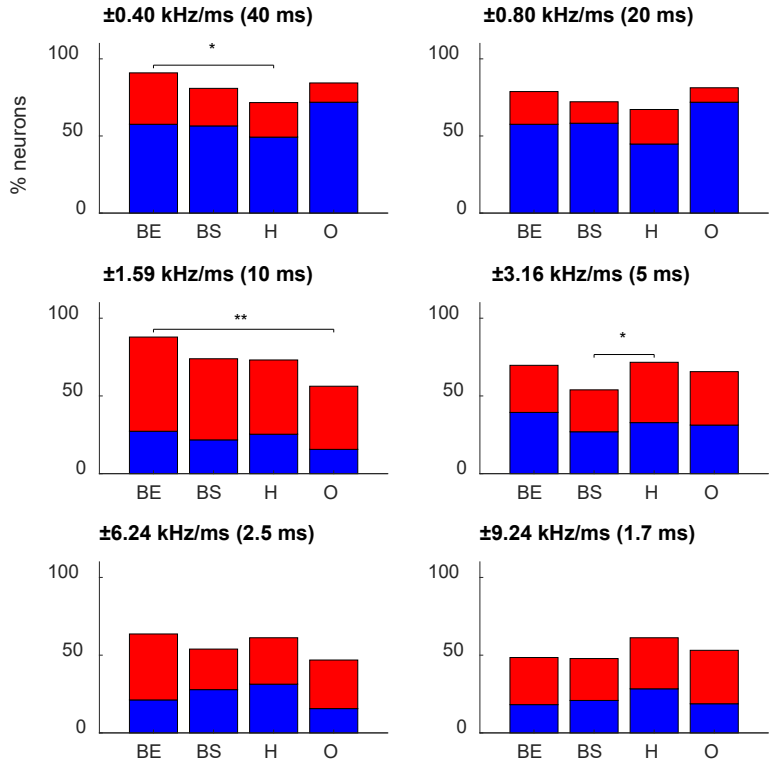

Figure 20 - Percent of direction selective neurons determined by ROC analysis for different MTF shapes, by aperiodic chirp duration (BE – Band-Enhanced, BS – Band-Suppressed, H – Hybrid, O – Other). In terms of chirp velocity, an aperiodic chirp of ±0.80 kHz/ms has a duration of 20 ms (equivalent to a SCHR chirp F0 of 50 Hz), ±1.59 kHz/ms has a duration of 10 ms (SCHR F0 100 Hz, etc.). Blue bar-segments correspond to upward-selective neurons, and red bar-segments correspond to downward-selective neurons. Brackets indicate significant differences of direction selectivity prevalence between groups, as determined by the χ^2 test of independence, with asterisks indicating the level of significance ($p < 0.05$, ** $p < 0.01$, *** $p < 0.001$). Precise p-values are reported here for each panel. ±0.40 kHz/ms (40 ms)—BE-H, $p = 0.0287$. ±1.59 kHz/ms (10 ms)—BE-O, $p = 0.0044$. ±3.16 kHz/ms (5 ms)—BS-H, $p = 0.0183$.*

CF was not strongly related to the prevalence nor the direction of aperiodic chirp selectivity (Fig. 11). Instead, prevalence of direction sensitivity in all CF groups decreased with increasing chirp velocity. Also, neurons were more commonly selective for downward chirps at higher chirp velocities.

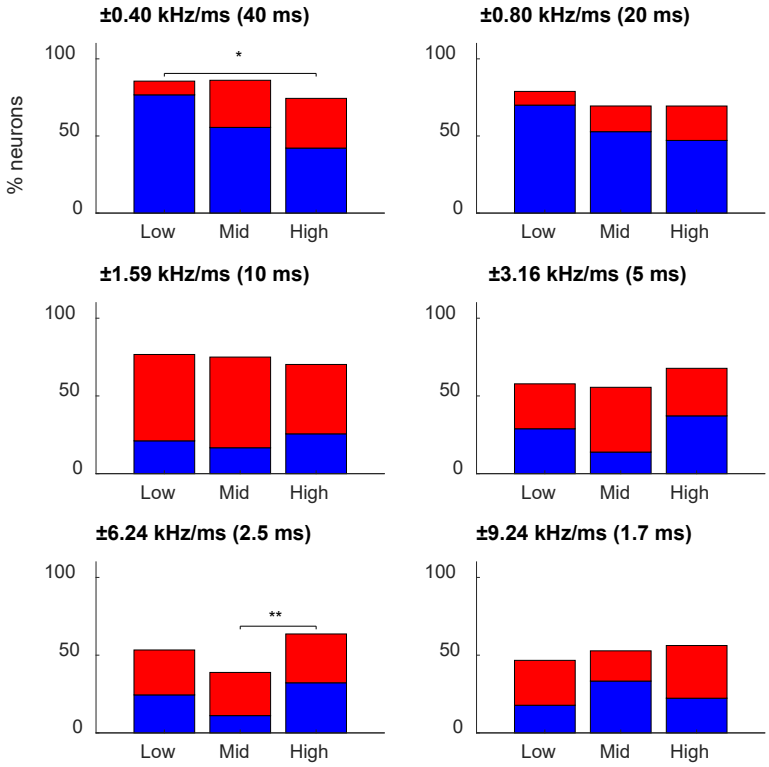

Figure 11 - Percent of direction selective neurons determined by ROC analysis for different CF ranges, low (<3 kHz), mid (>3 kHz and <6 kHz), and high (>6 kHz), by aperiodic chirp. In terms of chirp velocity, an aperiodic chirp of ±0.80 kHz/ms has a duration of 20 ms (equivalent to a SCHR chirp F0 of 50 Hz), ±1.59 kHz/ms has a duration of 10 ms (SCHR F0 100 Hz, etc.). Blue bar-segments correspond to upward-selective neurons, and red bar-segments correspond to downward-selective neurons. Brackets indicate significant differences of direction selectivity prevalence between groups, as determined by the χ^2 test of independence, with asterisks indicating the level of significance ($p < 0.05$, ** $p < 0.01$, *** $p < 0.001$). Precise p-values are reported here for each panel. ±0.40 kHz/ms (40 ms)—Low-High, $p = 0.0481$. ±6.24 kHz/ms (2.5 ms)—Mid-High, $p = 0.0083$.*

3.6. RVFs were often direction selective at slower-velocities and direction-insensitive at higher-velocities

As demonstrated by the ROC analysis performed on aperiodic chirp responses, direction selectivity to aperiodic chirps is commonplace. However, this analysis only addressed selectivity between direction of chirp-pairs and not sensitivity to chirp velocity. While RVFs reveal velocity tuning to aperiodic chirps for individual neurons (Figs. 3-7), further analysis is needed to

characterize trends in velocity tuning for the population of neurons. In order to identify the most common RVF characteristics, principal component analysis (PCA) was performed on the set of RVFs obtained from each single-unit. This approach reduced the dimensionality of the RVF dataset, and extracted the principal components, or the features that explained the most variability in the population.

Figure 12 shows the first three principal components, which together explained 74.0% of the variance in the data. Principal component 1 (PC1) had relatively high weights across high-magnitude velocities, showing that rate responses to high-velocity chirps tended to be positively correlated, regardless of direction. In other words, neurons responded similarly to either direction of high-velocity chirp. PC1 explained 48.5% of variance in the RVF data. Principal component 2 (PC2) had high weights at low-magnitude velocities, showing that rate responses to low-velocity chirps also tended to be positively correlated, regardless of direction. PC2 explained 13.8% of variance in the data. Finally, PC3 had large positive weights at slow upward velocities and negative weights at slow downward velocities, demonstrating that responses to upward and downward velocity chirps tended to be negatively correlated at slow velocities. PC3 was the main PCA dimension reflecting direction selectivity. PC3 explained 11.7% of variance in the data.

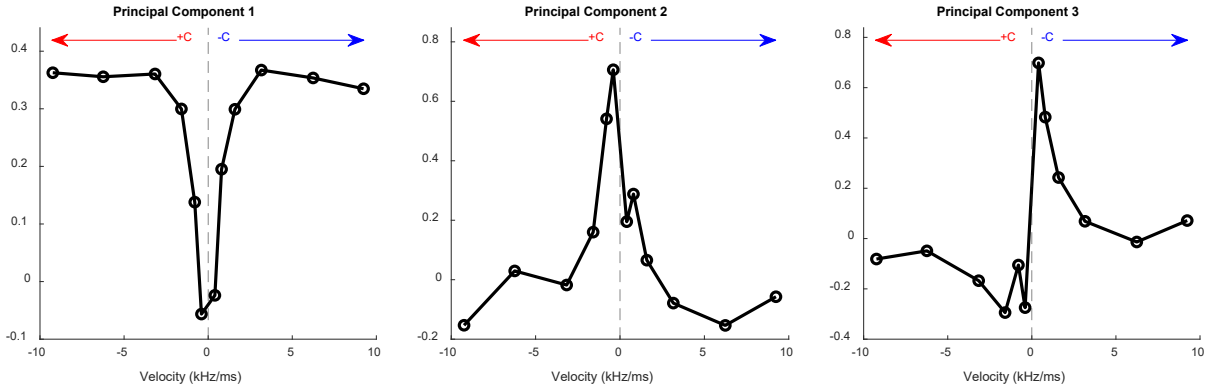

Figure 12 – Principal components derived from the set of RVFs (left, PC1; center, PC2; right, PC3). Y-axes reflect principal-component weights and are unitless.

The shapes of the first three principal components of the RVF data suggest that the most salient features of a neuron's RVF were its responses to high- and low-velocity chirps, rather than the direction of those chirps. However, PC3 showed that the direction selectivity of neurons for low-velocity chirps was an important feature of these datasets—however, PC3 primarily represented low-velocity chirp direction selectivity, consistent with the observation that chirp-direction selectivity at high-velocities was not as common. Instead, neural responses to chirps of high velocities tended to depend on chirp speed rather than on direction.

Principal component scores provide a measurement of how well each neuron's RVF aligns with the principal components in Fig. 12, and thus are a useful way to divide the population based on type of velocity sensitivity. This approach also allowed a comparison of velocity sensitivity against other response properties, such as MTF type and CF. As shown in Fig. 13, there was not a clear relationship between the scores of principal components 1-3 and either MTF type (symbol shapes) or CF (symbol colors). Furthermore, based on the three scatter plots in Fig. 13, there were no clusters of neurons based on principal-component analysis – that is, RVF subgroups were not revealed by this analysis. This suggests that a neuron's RVF is not directly related to its MTF or CF.

3.7. Velocity cues facilitated predictions of SCHR rate

Starting from the premise that responses to SCHR stimuli are dependent on AM (periodicity) tuning and/or velocity tuning, we used MTFs and RVFs to predict SCHR responses using a GLM. Figure 14 shows a visualization of this strategy on an example neuron (R24TT2P8N4, also depicted in Fig. 4). The neuron's SCHR response is shown as a surface plot on periodicity-velocity axes; darker colors correspond to higher response rates. This neuron responded more strongly to lower F0s and to downward SCHR (Fig. 14A). The color bars above and to the left

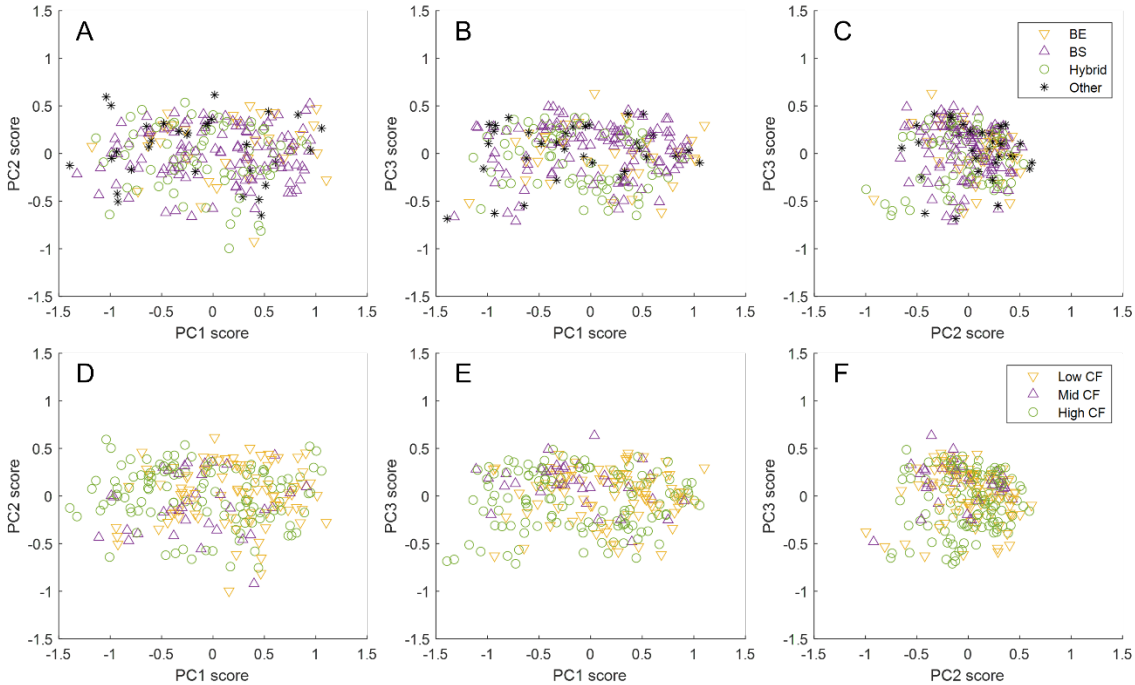

Figure 13 – Scatter plots depicting the Principal Component scores of each neuron, organized by MTF shape (A-C) and CF range (D-F). (A and D, PC2 vs PC1; B and E, PC3 vs PC1; C and F, PC3 vs PC2). In the top row (A-C), BE neurons are represented by yellow up-pointing triangles, BS neurons by purple down-pointing triangles, hybrid neurons by green circles, and other MTF shapes by black asterisks. In the bottom row (D-F), Low-CF neurons are represented by yellow up-pointing triangles, mid-CF by purple down-pointing triangles, and high-CF by green circles.

of the SCHR surface are the MTF and RVF of the neuron, respectively, and describe how the neuron's response rate depended on periodicity or velocity alone. Using a weighted combination of these two responses, the GLM predicted the SCHR response (Fig. 14B). By fitting an equation that included both periodicity and velocity terms (Eqn. 1), an accurate prediction of the recorded SCHR data was made ($R^2 = 0.98$). Removing either the periodicity or velocity terms reduced the quality of the prediction (Fig. 14C, D) (note that their interaction will be examined below). Predicting the SCHR response using the periodicity-only model (Eqn. 2) resulted in the disappearance of the distinct direction selectivity at lower F0s (Fig. 14C). Notably, a model using only periodicity tuning could not explain the observed direction selectivity. Conversely, a

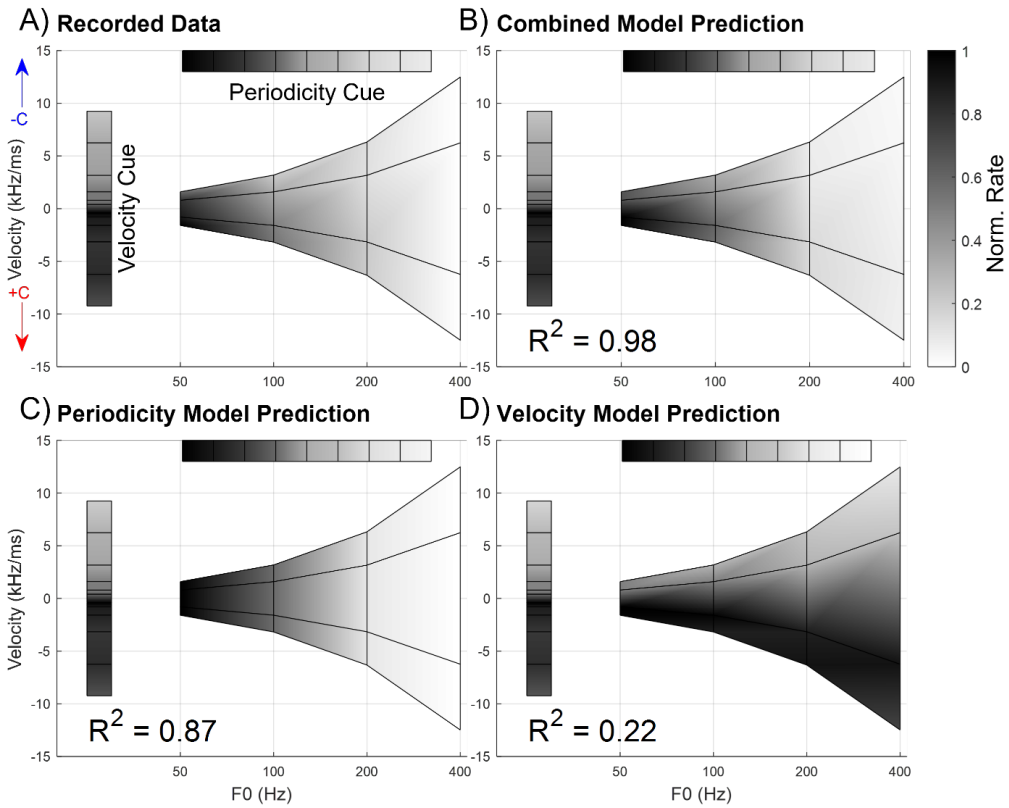

Figure 14 – GLM prediction of SCHR rates for an example neuron (R24TT2P8N4; same neuron as in Fig. 4). (A) SCHR rates plotted in Periodicity-Velocity space (center surface). Each of the 16 points on the surface plot correspond to an individual SCHR F0/C-value combination – for instance, four points have a SCHR F0 of 50 Hz. Their velocities vary with C-value; the points' C-values, from top to bottom, are -0.5, -1, 1, 0.5. This surface plot demonstrates the effect of C-value on chirp velocity. The periodicity cue and velocity cue are plotted alongside the SCHR surface plot—these are the MTF and RVF, respectively. The modulation frequency range of the MTF was limited to the section relevant to the range of SCHR F0s (50 – 400 Hz). Rate is marked using color, with darker shades indicating larger rates. The rate scale of each surface plot is separately normalized by its own maximum rate—thus, shading does not reflect absolute rates. Surface plot colors are interpolated. (B) SCHR rates predicted using the combined GLM equation (Eqn. 1), which uses both periodicity and velocity cues. Coefficient of determination (R^2) between predicted and recorded SCHR rates is also shown. (C) SCHR rates predicted using the periodicity-only GLM equation (Eqn. 2), and corresponding R^2-value. (D) SCHR rates predicted using the velocity-only GLM equation (Eqn. 3), and corresponding R^2-value.

prediction of the SCHR responses using the velocity-only model (Eqn. 3) explained a relatively small amount of variance in the data ($R^2 = 0.25$). This neuron was typical in that more variance in the data was explained by the periodicity-only model than by the velocity-only model. However, this neuron was also typical in that the velocity terms contribute a substantial

percentage of the variance explained by the combined model, as compared to the periodicity-only model.

The RVF in Fig. 14 had a higher response rate for downward aperiodic chirps. However, this neuron was only selective for downward SCHR at low F0s. Figure 15 shows how the velocity cue was used differently by the combined GLM model depending on periodicity. For aperiodic chirp velocities that closely matched the velocities of SCHR chirps with F0 equal to 50 Hz, a large change in chirp rate was associated with a high predicted SCHR rate (blue line). For higher F0s, aperiodic chirp rate had a smaller impact on the predicted SCHR rate, with slopes approaching zero (200- and 400-Hz lines, yellow and purple). Therefore, despite the RVF suggesting a strong selectivity for downward sweeps at all velocities, Fig. 15 shows that the

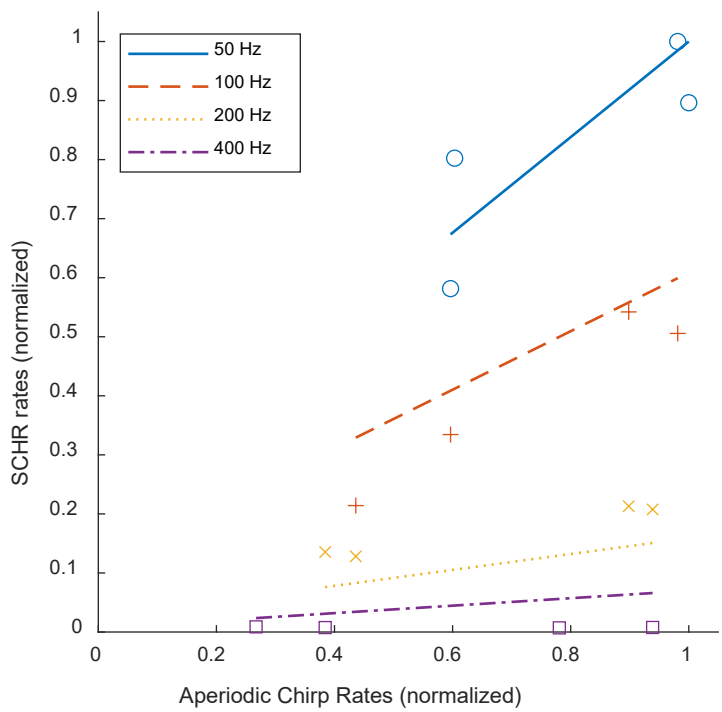

Figure 15 – SCHR rates vs aperiodic chirp rates (velocity cue) of unit R24TT2P8N4 plotted as recorded data (scatter plot) and GLM-fitted lines (solid lines). Blue solid line and circles correspond to 50 Hz, orange dashed line and plus signs correspond to 100 Hz, yellow dotted line and crosses correspond to 200 Hz, and purple dash-dotted line and squares correspond to 400 Hz. Both SCHR and aperiodic chirp rates are normalized by their own maximum rate. This example neuron is also shown in Figs. 4 and 14.

interaction between velocity and periodicity sensitivities drove the SCHR response rates. The importance of velocity-periodicity interaction illustrated in Fig. 15 was typical of many neurons in the study.

Using the method outlined in Fig. 14, an R^2 value was obtained for each of the three GLM models (Eqns. 2-4) by comparing predictions to neural responses. The contribution of velocity terms to the total explainable variance was calculated as a percentage, using Eqn. 4. Figure 16 shows this percentage versus the variance explained by the combined model. Many symbols are clustered around the *x*-axis, indicating that the contribution of velocity was not the primary determinant of SCHR rate and that periodicity tuning was the more important feature in predicting SCHR responses for these neurons. However, for neurons with a high total variance explained by the combined model (80-100%), the average contribution of velocity terms was about 20% and ranged up to about 50%. Figure 14 shows an example of such a neuron with high total explainable variance; the relatively small contribution of velocity to the predictions was not insubstantial because it necessarily contained all information about direction selectivity, a

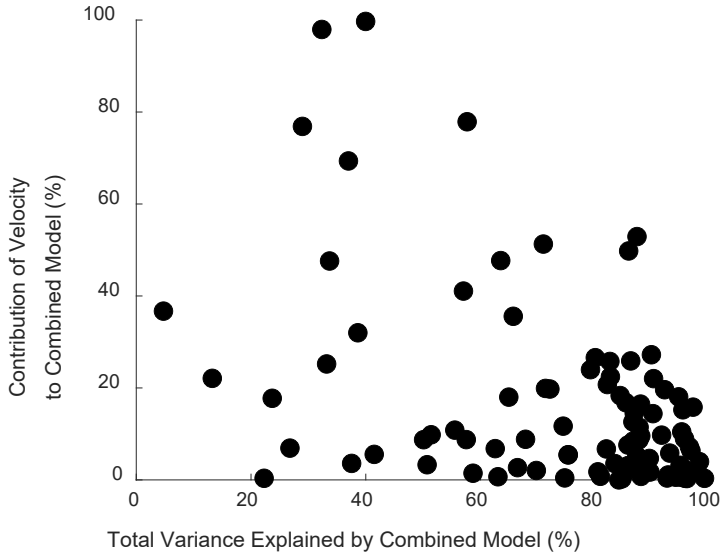

Figure 16 - Percent contribution of the velocity terms to the total explainable variance by the combined model vs. variance explained by the combined model.

cue for which the example unit was clearly sensitive (Fig. 4D, RVF). Furthermore, for many neurons with relatively low (20-60%) total explainable variance, the contribution of the velocity terms explained over 50% of the explained variance, suggesting that velocity cues were important predictors of these SCHR responses, perhaps more so than the relatively weaker periodicity predictor.

In summary, direction selectivity between SCHR pairs could not be explained with a model using periodicity alone. Because SCHR-direction selectivity was common (90.5%, Table 1), most IC neuron responses were necessarily influenced by velocity sensitivity.

4. Discussion

This study demonstrated the diversity of sensitivity to the velocity of fast frequency chirps in the IC, for the first time in an awake-rabbit model. Using ROC analysis, IC neurons were shown to be commonly selective for SCHR chirp direction, with 90.5% of neurons surveyed showing selectivity in at least one SCHR condition (Table 1). Neurons were also commonly selective for direction of aperiodic chirps, with 99.6% of neurons showing selectivity in at least one velocity-pair (Table 2). This study also showed that individual neurons had a wide variety of rate-response profiles which were described using RVFs. RVFs revealed that neurons were more commonly direction selective to chirps of lower velocities and responded to higher velocities in a direction-insensitive way. Finally, GLM analysis showed that SCHR rates could be accurately reconstructed using the periodicity and velocity sensitivity reflected in MTFs and RVFs, respectively. The combination of both velocity and periodicity cues was necessary to achieve the best predictions.

A common use of Schroeder-stimuli has been as a masker in psychophysical experiments evaluating detection of an increment in tone level. Notably, there is an impact of Schroeder-phase on the effectiveness of SCHR as a masker, with up to 20-dB lower thresholds

(less masking) for downward SCHR maskers than for upward SCHR maskers (Smith et al., 1986). An explanation from the literature attributes this effect to asymmetry of filtering in the cochlea—phase-dispersive properties of the basilar membrane (BM) result in a peakier response profile for downward than for upward SCHR, which is then compressed at the output of the cochlea, resulting in higher average energy in upward SCHR BM responses compared to downward SCHR, and thus more effective masking by upward SCHR stimuli (Recio and Rhode, 2000; Summers et al., 2003). This logic can also be applied to explain rate-differences between SCHR chirp directions. However, the results here suggest that other factors underlie the widespread chirp selectivity of IC single-units observed in this study. First, the phase-dispersion of the BM depends on CF, with neural masking differences observed primarily for CFs > 3-4 kHz (Recio, 2001). In this study, no consistent differences were observed in either the prevalence or direction of chirp selectivity between low-CF (< 3 kHz) and mid- or high-CF (> 3 kHz) neurons, in either SCHR or aperiodic chirp rates (Figs. 9, 11). Secondly, the cochlear dispersion hypothesis can only explain SCHR selectivity towards upward SCHR; despite this, neurons in the mid-to-high-CF range (> 3 kHz) could be selective for either direction of SCHR chirp (Fig. 9), suggesting that cochlear phase-dispersion was not the basis of IC chirp sensitivity. Similarly, Henry et al. (2022) found diverse SCHR selectivity in the IC of budgerigars (parakeet), though a statistical gradient was observed from upward SCHR selectivity at CFs below 2-3 kHz to downward SCHR selectivity for higher CFs. These findings were also consistent with a recent study in gerbils (Steenken et al., 2022) which reported that average rates of AN fibers could not explain behavioral discrimination of SCHR stimuli in gerbils, whereas temporal analyses of AN responses over short time (1-ms) windows could explain behavioral thresholds. Low correlations of AN rate to behavior provides further evidence against cochlear phase-dispersion driving IC selectivity. On the other hand, the presence of information for SCHR direction discrimination in the relatively fine timing of AN fibers is consistent with neural mechanisms that combine temporal information across frequency channels.

A potential mechanism to explain the diverse chirp-response profiles seen in this study may be found in IC inhibition. IC neurons receive excitatory and inhibitory inputs with varying frequencies and latencies that may interact to produce chirp selectivity (Pollak et al., 2011). Interactions between excitatory and inhibitory inputs varying in latency have long been implicated in mechanisms for frequency-sweep selectivity in bats (Suga, 1965; Fuzessery and Hall, 1996; Gordon and O'Neill, 1998). These mechanisms broadly are dependent on sideband inhibitory regions in excitatory tuning curves and the resulting asymmetry of responses to upward and downward frequency sweeps. Although not directly observed for all neurons, response map inhibition did not reliably predict chirp-direction selectivity among neurons for which inhibition was observed (e.g. Fig. 3), suggesting that sideband inhibition is not the sole mechanism underlying selectivity. To more comprehensively assess the effect of inhibition on chirp sensitivity, inhibition in the IC could be assessed by measuring response maps using pure tones in background noise – this would be an interesting direction for a future study.

A related mechanism for chirp selectivity based on dendritic filtering was proposed by Rall (1969) who included excitatory inputs organized spatially by frequency. In Rall's framework, a sweep that activates distal dendrites first, and proximal dendrites later, would temporally sum and generate a large synaptic input. While the existence of such large dendritic fields has not been reported in the IC, this mechanism has been hypothesized to underlie the frequency-sweep direction selectivity of octopus cells in the posteroventral cochlear nucleus (Rhode and Greenberg, 1992; Pollak et al., 2011). Notably, octopus cells project to the ventral nucleus of the lateral lemniscus (VNLL), which provides inhibitory innervation to the IC (Adams, 1997; Vater et al., 1997; Winer et al., 1995). Thus, direction selectivity of octopus cells, by way of the VNLL, may explain chirp selectivity in the IC; in this scenario, responses to chirps in one direction would be inhibited by input from the VNLL and disinhibited by chirps in the opposite direction. The possibility that IC chirp sensitivity originates in octopus cells is particularly intriguing

because, like IC neurons, octopus cells display a diversity of chirp response profiles and can be selective to either upward or downward chirps (Lu et al., 2022). Note that Lu et al. (2022) suggested that the diverse chirp selectivity in octopus cells could be explained by sequence detection, with excitation determined by a sequence of inputs with both frequency-dependent delays and varied amplitudes, rather than by simple coincidence detection of inputs with frequency-dependent delays. Another possibility is that chirp selectivity may originate in stellate neurons of the cochlear nucleus, which have been noted to display strong upward SCHR selectivity (Recio, 2001). However, because IC neurons can be selective for either upward or downward (Figs. 8, 9), cochlear nucleus stellates cannot be the only source of chirp sensitivity, and may contribute in addition to other sources, such as octopus cells.

Sensitivity to the direction of fast frequency changes has also been evaluated using neural responses to stimuli with random spectrotemporal fluctuations. One example is the Dynamic Moving Ripple (DMR) stimulus described in Escabí and Schreiner (2002). Designed to mimic spectrotemporal modulations present in natural sounds, such as speech or animal vocalizations, the stimulus is composed of a bank of sinusoidal carriers with an imposed spectrotemporal envelope. DMR stimuli have been used to generate spectrotemporal receptive fields (STRFs), which describe how neural response properties vary over frequency and time. It should be possible to produce a DMR stimulus with ripple velocity equivalent to SCHR chirps by substantially increasing the velocity of frequency sweeps compared to the original DMR stimuli. Doing so would require careful co-modulation of the temporal and spectral modulation variables and selection of an appropriate temporal analysis window for computing the stimulus spectrogram, which would be necessary to generate temporally-informative STRFs. Such STRFs may provide additional clues for analyzing IC neurons' chirp tuning.

While the combined GLM with both periodicity and velocity cues was able to reproduce SCHR rate profiles of IC neurons, often with high accuracy, some predictions did not explain a

high percentage of the variance (Fig. 16), suggesting that additional factors shaping SCHR rate profiles have yet to be uncovered. One possible source of this discrepancy was a gradual change in rate over long (50 – 150 ms) durations—Fig. 3 shows an example in which rate gradually increased (100 Hz F0), and Fig. 7 shows an example in which rate gradually decreased (50 Hz F0, C = -1). These long-term effects may be attributable to the auditory efferent system, and cannot be captured in brief aperiodic chirp responses. Similar long-term changes in rate have been reported in response to other complex sounds, representing a possible direction for future research (Farhadi et al., 2021).

SCHR-chirp sensitivity in the IC suggests a mechanism that may influence midbrain-level encoding of speech. When speech sounds, or any animal vocalizations, are produced, resonances within the vocal tract act as second-order filters, introducing phase shifts between components of harmonic sounds (Klatt, 1980). In the same way that SCHR chirps are produced by the relative phases of harmonic components, vocalizations will contain chirp-like features to which IC neurons may be similarly sensitive. IC neurons in this study were sensitive to SCHR chirps and directions over a frequency range relevant to human speech. Close examination of IC responses to SCHR chirps may reveal a novel influence on midbrain responses that is relevant to neural coding of speech and other harmonic sounds. The interaction of periodicity tuning and frequency-sweep velocity sensitivity observed in this study would also influence responses to other complex harmonic sounds, such as those common in speech and music.

Acknowledgements

We acknowledge the assistance of Kristina S. Abrams, Johanna B. Fritzinger, and Dr. Swapna Agarwalla for help with physiological experiments. Supported by NIH-DC001641 and NIH-F31DC019816.

References

Adams JC (1997) Projections from octopus cells of the posteroventral cochlear nucleus to the ventral nucleus of the lateral lemniscus in cat and human. Aud Neurosci 3:335-350.

Andoni S, Li N, Pollak GD (2007) Spectrotemporal Receptive Fields in the Inferior Colliculus Revealing Selectivity for Spectral Motion in Conspecific Vocalizations. The Journal of Neuroscience 27:4882-4893.

Awan SN, Novaleski CK, Rousseau B (2014) Nonlinear Analyses of Elicited Modal, Raised, and Pressed Rabbit Phonation. Journal of Voice 28:538-547.

Casseday JH, Ehrlich D, Covey E (1994) Neural Tuning for Sound Duration: Role of Inhibitory Mechanisms in the Inferior Colliculus. Science 264:847-850.

Davis KA (2005) Spectral Processing in the Inferior Colliculus. In: International Review of Neurobiology, pp 169-205: Academic Press.

Egan JP, Egan JP (1975) Signal detection theory and ROC-analysis: Academic press.

Escabi MA, Schreiner CE (2002) Nonlinear spectrotemporal sound analysis by neurons in the auditory midbrain. Journal of Neuroscience 22:4114-4131.

Escabi MA, Miller LM, Read HL, Schreiner CE (2003) Naturalistic auditory contrast improves spectrotemporal coding in the cat inferior colliculus. Journal of Neuroscience 23:11489-11504.

Farhadi A, Jennings SG, Strickland EA, Carney LH (2021) A Closed-Loop Gain-Control Feedback Model for The Medial Efferent System of The Descending Auditory Pathway. In: ICASSP 2021 - 2021 IEEE International Conference on Acoustics, Speech and Signal Processing (ICASSP), pp 291-295.

Fuzessery ZM (1994) Response selectivity for multiple dimensions of frequency sweeps in the pallid bat inferior colliculus. Journal of Neurophysiology 72:1061-1079.

Fuzessery Z, Hall J (1996) Role of GABA in shaping frequency tuning and creating FM sweep selectivity in the inferior colliculus. Journal of neurophysiology 76:1059-1073.

Gordon M, O'Neill WE (1998) Temporal processing across frequency channels by FM selective auditory neurons can account for FM rate selectivity. Hearing research 122:97-108.

Heffner H, Masterton B (1980) Hearing in Glires: Domestic rabbit, cotton rat, feral house mouse, and kangaroo rat. The Journal of the Acoustical Society of America 68:1584-1599.

Henry KS, Wang Y, Abrams KS, Carney LH (2023) Mechanisms of masking by Schroeder-phase harmonic tone complexes in the budgerigar (*Melopsittacus undulatus*). bioRxiv:2022.2010.2026.513930.

Kim DO, Carney L, Kuwada S (2020) Amplitude modulation transfer functions reveal opposing populations within both the inferior colliculus and medial geniculate body. Journal of Neurophysiology 124:1198-1215.

Klatt DH (1980) Software for a cascade/parallel formant synthesizer. The Journal of the Acoustical Society of America 67:971-995.

Krishna BS, Semple MN (2000) Auditory Temporal Processing: Responses to Sinusoidally Amplitude-Modulated Tones in the Inferior Colliculus. Journal of Neurophysiology 84:255-273.

Langner G, Schreiner CE (1988) Periodicity coding in the inferior colliculus of the cat. I. Neuronal mechanisms. Journal of Neurophysiology 60:1799-1822.

Levitt H (1971) Transformed up-down methods in psychoacoustics. The Journal of the Acoustical society of America 49:467-477.

Liberman AM, Mattingly IG (1989) A Specialization for Speech Perception. Science 243:489-494.

Lu H-W, Smith PH, Joris PX (2022) Mammalian octopus cells are direction selective to frequency sweeps by excitatory synaptic sequence detection. Proceedings of the National Academy of Sciences 119:e2203748119.

Nelder JA, Wedderburn RW (1972) Generalized linear models. Journal of the Royal Statistical Society: Series A (General) 135:370-384.

Nelson PC, Carney LH (2007) Neural Rate and Timing Cues for Detection and Discrimination of Amplitude-Modulated Tones in the Awake Rabbit Inferior Colliculus. Journal of Neurophysiology 97:522-539.

Pollak GD, Xie R, Gittelman JX, Andoni S, Li N (2011) The dominance of inhibition in the inferior colliculus. Hearing Research 274:27-39.

Rall W (1969) Time constants and electrotonic length of membrane cylinders and neurons. Biophysical Journal 9:1483-1508.

Recio A (2001) Representation of harmonic complex stimuli in the ventral cochlear nucleus of the chinchilla. The Journal of the Acoustical Society of America 110:2024-2033.

Recio A, Rhode WS (2000) Basilar membrane responses to broadband stimuli. The Journal of the Acoustical Society of America 108:2281-2298.

Rhode WS, Greenberg S (1992) Physiology of the cochlear nuclei. In: The mammalian auditory pathway: Neurophysiology, pp 94-152: Springer.

Schroeder M (1970) Synthesis of low-peak-factor signals and binary sequences with low autocorrelation (Corresp.). IEEE Transactions on Information Theory 16:85-89.

Schwarz DM, Zilany MSA, Skevington M, Huang NJ, Flynn BC, Carney LH (2012) Semi-supervised spike sorting using pattern matching and a scaled Mahalanobis distance metric. Journal of Neuroscience Methods 206:120-131.

Smith BK, Sieben UK, Kohlrausch A, Schroeder MR (1986) Phase effects in masking related to dispersion in the inner ear. The Journal of the Acoustical Society of America 80:1631-1637.

Steenken F, Oetjen H, Beutelmann R, Carney LH, Koeppl C, Klump GM (2022) Neural processing and perception of Schroeder-phase harmonic tone complexes in the gerbil: Relating single-unit neurophysiology to behavior. European Journal of Neuroscience 56:4060-4085.

Suga N (1965) Analysis of frequency-modulated sounds by auditory neurones of echo-locating bats. J Physiol 179:26-53.

Summers V, Boer Ed, Nuttall AL (2003) Basilar-membrane responses to multicomponent (Schroeder-phase) signals: Understanding intensity effects. The Journal of the Acoustical Society of America 114:294-306.

Vater M, Covey E, Casseday J (1997) The columnar region of the ventral nucleus of the lateral lemniscus in the big brown bat (Eptesicus fuscus): synaptic arrangements and structural correlates of feedforward inhibitory function. Cell and tissue research 289:223-233.

Whitehead ML, Lonsbury-Martin BL, Martin GK (1992) Evidence for two discrete sources of 2f1−f2 distortion-product otoacoustic emission in rabbit: I. Differential dependence on stimulus parameters. The Journal of the Acoustical Society of America 91:1587-1607.

Winer JA, Larue DT, Pollak GD (1995) GABA and glycine in the central auditory system of the mustache bat: structural substrates for inhibitory neuronal organization. Journal of Comparative Neurology 355:317-353.

Yin TCT, Smith PH, Joris PX (2019) Neural Mechanisms of Binaural Processing in the Auditory Brainstem. Compr Physiol 9:1503-1575.